Assessment of Seasonal Variations in GNSS Errors over UAE - Abu Dhabi Case Study

Abdulla Alnaqbi [1], M. M. Yagoub [2], Alina Hasbi [3]

[1]PhD student, Department of Geography and Urban Sustainability, UAE University; email: 202190029@uaeu.ac.ae

[2]Department of Geography and Urban Sustainability, UAE University; email: myagoub@uaeu.ac.ae

[3]National Space Science and Technology Center, UAE University; email: alina.hasbi@uaeu.ac.ae

Keywords: Global Navigation Satellite Systems, Differential Positioning, IGS, Continuous Operating Reference Stations, Precise Point Positioning (PPP)

Abstract

Global navigation satellite systems (GNSS) play a vital role in daily applications. This includes precise surveying and mapping, platform navigation by sea, land, and air, monitoring of large structural deformations, and recreational applications. However, the accuracy requirements vary from user to user based on their needs and applications. The accuracy of GNSS depends on numerous factors and is impacted by different error sources, such as tropospheric delay and ionospheric error, from the moment the signal leaves the GNSS satellite until it reaches the receiver antenna of the end user. These errors are classified into three major components: satellite, propagation, and receiver errors. This study assessed the seasonal variations in GNSS errors over Abu Dhabi in the United Arab Emirates. The analysis was based on historical continuous operating reference stations (CORSs) readings for 2018. Two different software were used to derive the final coordinates of two Abu Dhabi CORS stations observed for three days every month in 2018. The results indicated variations between -3 mm and 3 mm in the horizontal components and -16 mm and 12 mm in the vertical components for the Abu Dhabi station for all days of 2018. In contrast, the horizontal component of Madinat Zayed station varied between -2 mm and 4 mm and -8 mm and 9 mm in the horizontal and vertical components, respectively. The Positioning error was larger during summer than during winter; this may be primarily attributed to the ionospheric effect.

1. Introduction

Applications of global navigation satellite systems (GNSS) technology have been increasing continuously, influencing all aspects of our lives. Originally, GNSS was used in surveying and mapping applications in addition to navigation of ships, airplanes, and military vehicles. Currently, GNSS applications range from financial transactions that require precise timing to the sensing of the atmosphere for weather forecasting. Fernandes et al. (2015) integrated a GNSS-derived Path Delay with microwave radiometer measurements to obtain precise wet tropospheric correction for altimetric products. Awange (2012) used GNSS data for remote sensing of the atmosphere through the measurement of different physical variables, such as atmospheric temperature, pressure, and tropopause height, which are required for weather and climate change monitoring.

Satellite errors are primarily caused by the satellite orbit and clock errors onboard each satellite vehicle. However, these errors may vary temporally and cannot be eliminated completely owing to the different satellite orbits and clock types attached to different constellations (Shu et al., 2019). However, the type of satellite orbit and satellite clock hardware characteristics significantly contribute to the magnitude of the broadcast orbit and clock offset errors (Lou et al., 2014). Errors in signal propagation include GNSS signal delays as it travels through atmospheric layers, namely the troposphere and ionosphere. (Rizos, 1997). The Ionosphere is the upper part of the atmosphere, extending from 50 km to 1000 km above the Earth's surface (Hofmann-Wellenhof et al., 2008). This layer forms a challenging environment for different satellite technology applications such as communications, navigation, and surveillance (CNS). In this layer, gas molecules and atoms interact with ultraviolet and X-ray radiations coming from the sun, leading to a phenomenon called ionization (El-Rabbany, 2006). The physical and chemical properties of the ionosphere, including the quantity of ions and electrons, vary based on the solar and magnetic activity, geographic location, time of the day, and time of the year (Hong, 2008). Ansari et al. (2017) investigated variations in the total electron content (TEC) using the Turkish Permanent GNSS Network and found that the maximum TEC value was observed at 10.00 UTC and reached its minimum at midnight. The month of March witnessed the highest TEC concentration, followed by May and August, whereas the lowest value was recorded in September. The ionosphere is a frequency-dependent dispersive medium that accelerates the propagation of the carrier phase and slows down the code pseudorange measurement by the same amount (El-Rabbany, 2006). This error can be easily eliminated using a dual-frequency GNSS receiver by forming an ionosphere-free linear combination using measurements from the L1 and L2 frequencies. Positioning accuracy is directly proportional to the TEC along the signal travel path in the ionosphere and inversely proportional to the square of the signal frequency (Hofmann-Wellenhof et al., 2008). Ionospheric errors vary spatially and temporally based on the location of the observer and the time of the GNSS measurement.

This contribution has been peer-reviewed. The double-blind peer-review was conducted on the basis of the full paper.
https://doi.org/10.5194/isprs-annals-X-G-2025-87-2025 | © Author(s) 2025. CC BY 4.0 License.

Along with temporal changes in the ionosphere, the electron density also varies in cycles of approximately 11 years (Li et al., 2018). The incidence of solar activity is higher during these peaks, and the layers of the terrestrial atmosphere become more ionized. Further, increase in TEC values is directly proportional to the solar activity or the number of sunspots (Jerez and Alves, 2020).

The troposphere is located in the lower atmosphere. It extends from the Earth's surface to approximately 50 km and comprises dry gases and water vapor (Brunner and Welsch, 1993). In the GNSS applications, the effect of the troposphere and stratosphere is often referred as the "tropospheric effect" and considered one layer of 50 km height from the earth surface (Langley, 2011). Tropospheric delay is a function of temperature, pressure, and humidity along the signal propagation path. Because tropospheric refraction is frequency-independent, dual-frequency observations cannot be used to subtract it (Garrido et al., 2018). Hence, the troposphere delays GNSS carrier phase and code measurements by the same amount, resulting in longer satellite-to-receiver range measurements (Hofmann-Wellenhof et al., 2008).

The error in the measured geometric range can range from approximately 2.0 m to 2.6 m in the zenith direction and increase to approximately 20 m to 28 m near the horizon and at lower elevation angles (Sanlioglu and Zeybek, 2012). The delay is governed by the satellite elevation angle and altitude of the observer. Hence, signals from satellites at low elevation angles travel longer paths through the troposphere than those at higher elevation angles (Petropoulos and Srivastava, 2021). Therefore, the tropospheric delay is minimum at the user's zenith and maximum near the horizon (Brunner and Welsch, 1993). The tropospheric delay is divided into two components: the dry component (also known as hydrostatic) and wet component. The dry component, composed of Nitrogen gas N_2 and Oxygen O_2, accounts for approximately 90 % of the delay. In contrast, the wet component is composed of water vapor and is responsible for approximately 10 % of the remaining tropospheric delay (Hofmann-Wellenhof et al., 2008).

The total tropospheric delay introduced in the zenith direction is referred to as the zenith tropospheric delay (ZTD) and is the sum of the zenith hydrostatic delay (ZHD) and zenith wet delay (ZWD) (Astudillo et al., 2018). The dry part is highly predictable and can be modeled mathematically using empirical prediction models, whereas the wet part is difficult to model mathematically because of its high correlation with the water vapor content along the signal path, which varies both temporally and spatially. The most common empirical models used to date in GNSS positioning are the Saastamoinen and Hopfield models, which account for the dry component. Whereas, various mapping functions such as the Global Mapping Function (GMF) and Vienna Mapping Function (VMF) account for the wet component. The dry component is completely absorbed by the a priori model and the wet component is estimated using the troposphere zenith path delay (ZPD) parameters based on the selected mapping function (Garrido et al., 2018).
The tropospheric delay error can be significantly reduced by differentiating observations between sites with relatively short baselines. Uncertainty in modelling the troposphere degrades the accuracy of the height component and has a smaller effect on latitude and longitude (Rizos, 1997).

A noticeable improvement in positioning, navigation, and timing (PNT) has been achieved owing to the introduction of more GNSS constellations by various nations in addition to GPS and GLONASS, such as the Chinese BeiDou and European Galileo navigation satellite systems.
The study examines the seasonal variations in GNSS errors over Abu Dhabi, UAE using historical data from two continuous operating reference stations (CORSs) for 2018. Several studies have attempted to evaluate the positioning accuracy of continuous operating reference station (CORS) networks globally to characterize seasonal variations in the computed coordinates. Łyszkowicz et al. (2021) used the GipsyX software to analyze permanent stations data in Poland for 8 years (2011–2018) to determine the Earth's crust movements. In their study, the PPP technique was adopted to process multi-GNSS observations to determine the variation in the horizontal and vertical movements of the Earth's crust over 8 years. Their results indicated variations in the horizontal component in the range of 11.3 mm to 21.6 mm, and from -0.6 mm to 3.7 mm in the vertical component. Further, they found that processing multi-GNSS observations using all available systems improved the accuracy of the computed station coordinates, even with a shorter time interval of data, when compared to using a single satellite navigation system (e.g., GPS) alone. Jerez and Alves (2020) assessed the positioning performance of GPS/GLONASS observations using six GNSS stations from the Brazilian Network for Continuous Monitoring (RBMC) using the Canadian Spatial Reference System PPP (CSRS-PPP) method. Their results demonstrated more errors owing to ionospheric errors in October, whereas the lowest error was observed in June owing to lower ionospheric activity in that region during this period. The objective of this study was to assess the seasonal variation in errors for two GNSS CORSs in Abu Dhabi in 2018. The assessment was based on daily, monthly, semiannual, and annual data. The ultimate goal was to determine whether errors varied in space and time during the year in this region. To the best of our knowledge, this is the first such study to be conducted in Abu Dhabi, thereby, filling an existing gap in the literature. Only data from two stations in 2018 were available to the authors. Because the study is exploratory in nature, the data provides clues about the general trend of seasonal change in errors. A study conducted by (Khoptar and Savchuk, 2020) used one station data spanning two years' data in Poland. This assessment will contribute to the advancement of GNSS technology by providing valuable insights into the factors driving seasonal variations in positioning errors. Moreover, the findings of this study will have practical implications for various applications that rely on precise GNSS positioning, such as precision agriculture, geospatial mapping, and infrastructure monitoring. By addressing seasonal variations in GNSS errors, we can improve the performance and reliability of these applications, leading to more efficient and accurate data collection and analysis.

2. Methodology

In this study, the observation data files in the RINEX format for the two CORS stations were provided by the municipality of Abu Dhabi and used for analysis. The data were logged for 24 h at a sampling rate of 1 s and an elevation cutoff angle of 7.5°. The data were logged at both the L1 and L2 frequencies for the GPS and GLONASS constellations. The days chosen for this assessment were the 1st, 15th, and 28th of each month from January to December 2018. The stations selected for this analysis

were distributed within the Abu Dhabi Emirate, as shown in Figure 1. The distance between the stations was 95 km and the stations were located under different environmental conditions. The Abu Dhabi station (ADCN) is located within the city and is closer to the coast than the Madinat Zayed station (MDZN).

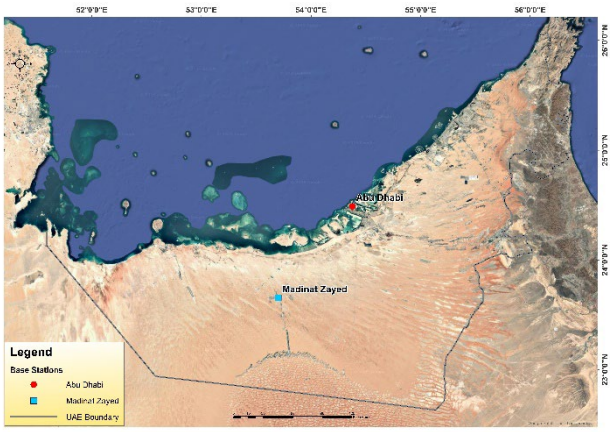

Figure 1. Location of the GNSS Continuous Operating Reference Stations (CORSs)

The observation data files were processed in the differenced and non-differenced modes using different applications. Station coordinates in the differential positioning mode were computed using the Trimble Business Center (TBC) software. TBC utilizes IGS products to compute precise coordinates based on the International Terrestrial Reference Frame (ITRF). The observation data files for the selected IGS reference stations covering 2018, along with the final orbits and precise clocks, were downloaded from the IGS website (IGS, 2018). The days chosen for this assessment were days 001, 015, 028, 032, 046, 059, 060, 074, 087, 091, 105, 118, 121, 135, 148, 152, 166, 179, 182, 196, 209, 213, 227, 240, 244, 258, 271, 274, 288, 301, 305, 319, 332, 335, 349, and 362 of the year 2018. The previous days were selected to represent the daily, and monthly variations in GNSS errors. The justification for this selection was to investigate seasonal variations in the estimated coordinates for each station using two different methods (Isioye et al., 2019). Selecting three observation days each month for a year to assess the GNSS errors over a certain area is a common practice in GNSS data analysis (Dogan, Uludag, & Demir, 2014). This approach facilitates a good representation of the different atmospheric and environmental conditions that affect GNSS signals. This is because GNSS accuracy is affected by various factors, such as satellite geometry, ionospheric activity, and receiver noise, which can vary with time. By selecting three observation days each month for a year, the data can capture the temporal variations in these factors and provide a more accurate assessment of GNSS errors over the area. However, by collecting data on different days and times, the variations in ionospheric and tropospheric conditions, which play a vital role in GNSS measurement performance, can be incorporated. The CSRS-PPP version 3.50.2, developed by the Geodetic Survey Division of Natural Resources of Canada (NRCan), was used to compute the three positioning components for both stations in the undifferenced mode. CSRS-PPP uses a dynamic filter to estimate station positions in static or kinematic mode, station-clock states, local tropospheric zenith delays, and carrier-phase ambiguities (NRCan, 2020).

In this study, different time series of GNSS observations were created for each station to achieve robust results. First, the entirety of the 36 RINEX observation files was analyzed for each station covering the entire year of 2018, with three days representing each month. In the second phase, three different time series were created, representing the observation on the 1st, 15th, and 28th days of the month. The objective was to generate the overall trends of the accuracy variations and subsequently assess how the variation in the accuracy over the same day for different months of observations.

3. Results and Discussion

In this study, different variants of both the station's time series were generated using the TBC and CSRS-PPP techniques and compared. The time series of the positioning components differences (delta Northing, delta Easting, and delta Height) between the reference values and individual reading were computed and the trends for each component are presented in the Figures. First, the three-dimensional GNSS differential positioning coordinates for both stations were derived, which were referenced to the IGS realization of the ITRF2014 reference frame computed using TBC software. The computed standard deviations for ADCN were 0.0090 m and 0.0092 for the northern and eastern components, respectively, while the standard deviation of the ellipsoidal height was 0.0061 m. Whereas, the computed standard deviations for MDZN were 0.0102 m and 0.0090 for the northern and eastern components, respectively, while the standard deviation of the ellipsoidal height was 0.0048 m. The reported statistics indicated that all three components were less than 15 mm in the minimal accuracy required for the establishment of a geodetic reference station (Ebner and Featherstone, 2008).
Figures 2 and 3 present the positioning errors in northing, easting, and ellipsoidal height for ADCN station computed by TBC and CSRS-PPP for all 36 observation files (DOY 1 to DOY 362).

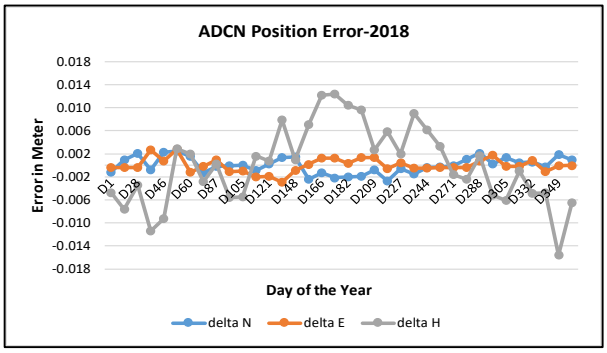

Figure 2. Positioning Errors in ADCN station for all DOY (2018) computed by TBC

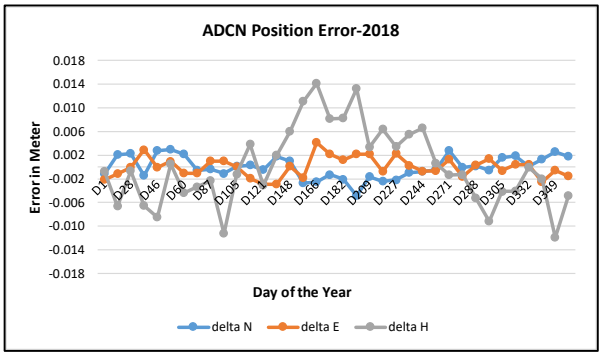

Figure 3. Positioning Errors in ADCN station for all DOY (2018) computed by CSRS-PPP

Using TBC differential processing, the error in the northern component ranged from -3 mm to 2 mm, the eastern component ranged from -3 mm to 3 mm. Further, and the ellipsoidal height exhibited the largest error, as expected, ranging from – 16 mm to 12 mm. Similarly, the positioning error derived by the CSRS-PPP processing ranged from -5 mm to 3 mm for the northern error, the easting error ranged from -3 mm to 4 mm and the ellipsoidal height ranged from -12 mm to 14 mm. It is clear that the error in the height component was larger than that in the horizontal component, which aligns with the specifications of the GNSS accuracy performance (US- Department of Defense, 2020). The height component was largely influenced by the unresolved residual of the wet tropospheric component. Figure 4 shows the standard deviations of the computed differences for both stations using TBC and CSRS-PPP. The results confirmed the robustness of the collected observations and processing techniques used in this study. The solution derived using the differential technique with the TBC was slightly better than that derived using PPP. This could be explained by the fact that most of the errors were removed using differential processing, particularly tropospheric and ionospheric errors, resulting in a robust ambiguity resolution compared to the precise positioning technique.

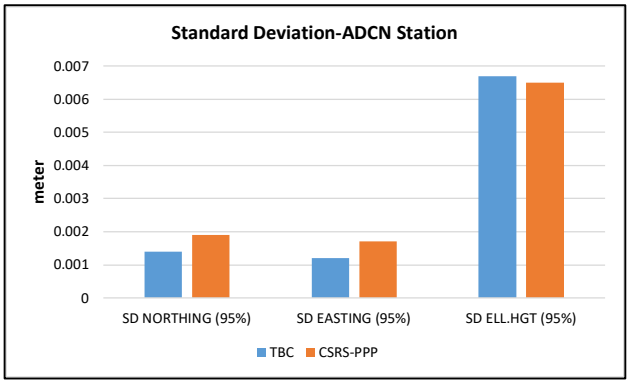

Figure 4. Standard Deviations for TBC and CSRS-PPP Solutions (ADCN station)

Figure 5 shows the accuracy variations of the time series for the 1st day of the month for ADCN station, with a total of 12 elements representing the entire year of 2018.

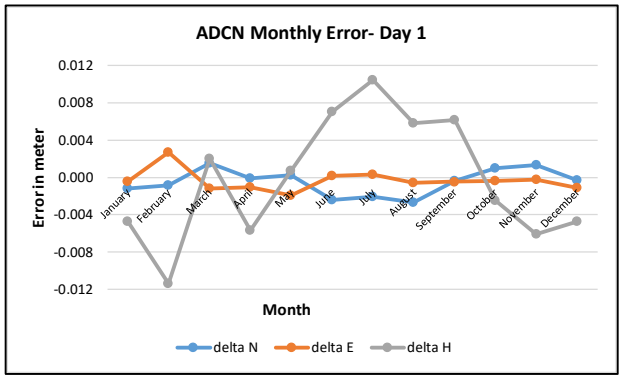

Figure 5. Positioning Errors in ADCN station for 1st day of the month (2018) computed by TBC

The maximum error was apparent in the months of February, July, and August, particularly in the height component, whereas the minimum error was observed in March, May, and October. Furthermore, the error in the horizontal component was very low and stable over the entire year, confirming the robustness of the data used and processing techniques. Figure 6 shows the accuracy variations of the time series for the 15th day of the month, with a total of 12 elements representing the entire year of 2018. By comparing graphs 5, 6, and 7 we can notice a large decrease in the height error component for the month of February, that reached 12 mm at the first day of the month and reached 4 mm at the end of the month.

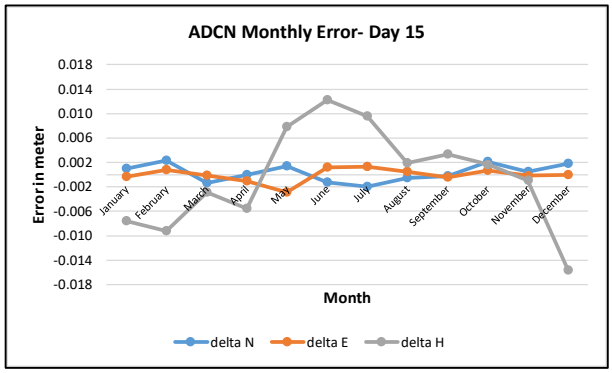

Figure 6. Positioning Errors in ADCN station for 15th day of the month (2018) computed by TBC

Figure 7 shows the accuracy variations of the time series for the 28th day of the month, with a total of 12 elements representing the entire year of 2018.

This contribution has been peer-reviewed. The double-blind peer-review was conducted on the basis of the full paper.
https://doi.org/10.5194/isprs-annals-X-G-2025-87-2025 | © Author(s) 2025. CC BY 4.0 License.

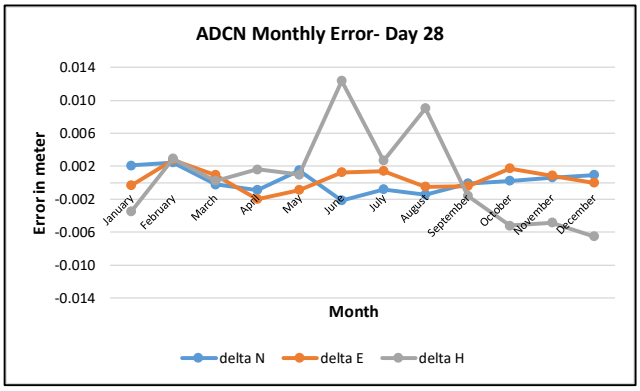

Figure 7. Positioning Errors in ADCN station for 28th day of the month (2018) computed by TBC

The error in the northern component for MDZN station ranged from -2 mm to 3 mm, while the eastern component error ranged from -2 mm to 4 mm, and the ellipsoidal height exhibited the largest error, as expected, ranging from – 8 mm to 9 mm using differential processing by TBC software, as depicted in Figure 8.

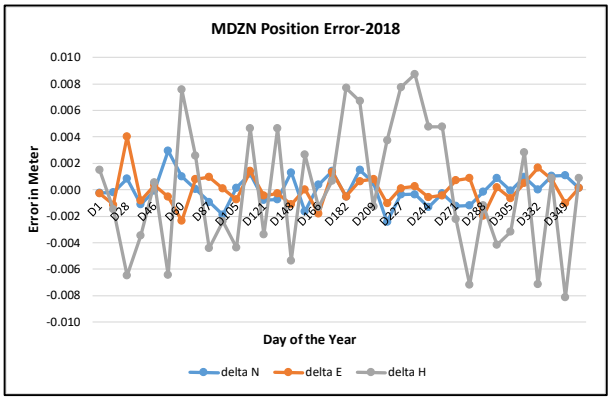

Figure 8. Positioning Errors in MDZN station for all DOY (2018) computed by TBC

Similarly, the positioning northing error derived by the PPP processing ranged from -3 mm to 2 mm, the eastern error ranges from -3 mm to 3 mm, and the ellipsoidal height ranged from -16 mm to 12 mm as shown in Figure 9.

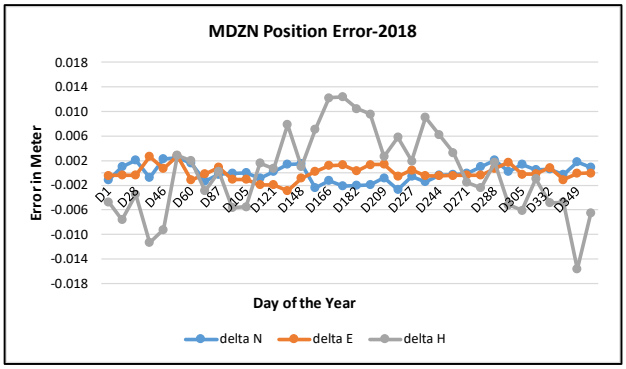

Figure 9. Positioning Errors in MDZN station for all DOY (2018) computed by CSRS-PPP

Figure 10 shows the standard deviations of the computed differences for MDZN station using TBC and CSRS-PPP. These results confirmed the robustness of the collected observations and processing techniques used in this study. The solution derived using the differential technique with the TBC was slightly better than that derived using PPP.

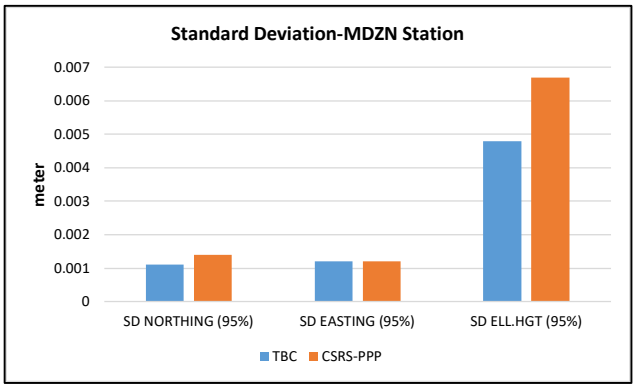

Figure 10. Standard Deviations for TBC and CSRS-PPP Solutions (MDZN)

Figure 11 shows the accuracy variations of the time series for the 1st day of the month for MDZN station, with a total of 12 elements representing the entire year of 2018. The graph shows that the maximum error occurred in March, July, and October, primarily in the height component, whereas the minimum error occurred in January, April, and December.

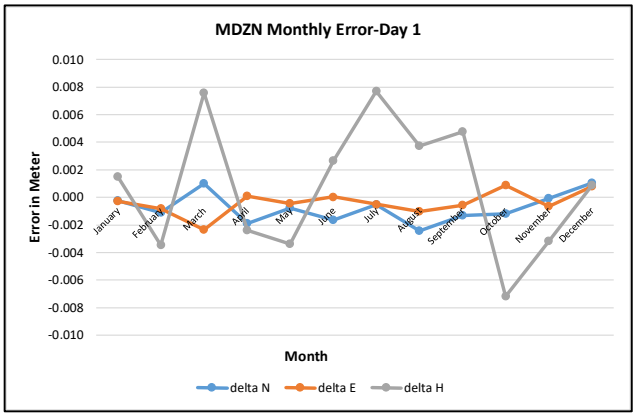

Figure 11. Positioning Errors in MDZN station for 1st day of the month (2018) computed by TBC

Figure 12 shows the accuracy variations of the time series for the 15th day of the month, with a total of 12 elements representing the entire year of 2018. The maximum error was obtained in July, August, and December, whereas the minimum error appeared in January, February, June, and October.

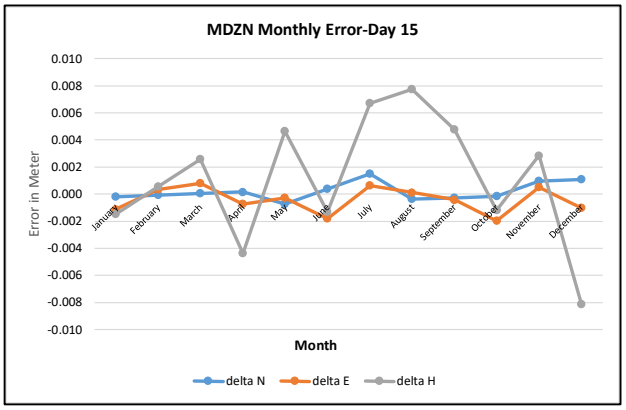

Figure 12. Positioning Errors in MDZN station for 15th day of the month (2018) computed by TBC

Figure 13 shows the accuracy variations of the time series for the 28th day of the month, with a total of 12 elements representing the whole year 2018. The maximum error was obtained in January, February, August, and November, whereas the minimum error appeared in June, July, and December.

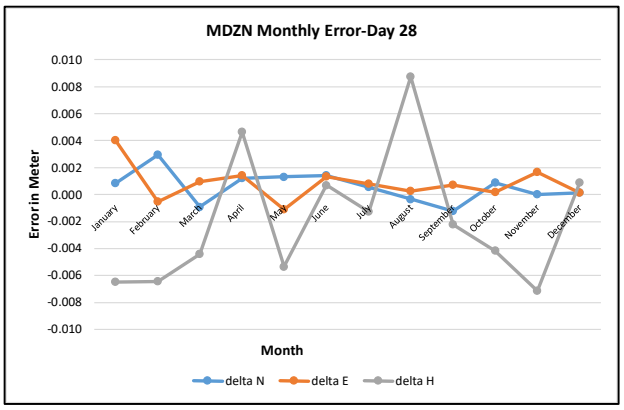

Figure 13. Positioning Errors in MDZN station for 28th day of the month (2018) computed by TBC

Figure 14 shows the error variation for ADCN station in three different observation windows in February and August 2018. As evident, the accuracy of all three components was better in February than in August, except for the height value observed between 7 am and 9 am in February. This can be attributed to the unresolved residual of the wet component of the tropospheric error. Furthermore, the graph shows that the maximum positioning error was observed in the morning window in both months of the year.

Figure 14. Hourly Error for ADCN station (February & August 2018)

Figure 15 shows the error variation for MDZN station for three different observation windows in February and August, 2018. As evident, the accuracy of all three components was better in February than in August, except for the northern component observed between 7 am and 9 am in February. From both comparisons, we conclude that the ionospheric impact was greater in August than in February, leading to larger errors in the positioning accuracy of both stations.

This contribution has been peer-reviewed. The double-blind peer-review was conducted on the basis of the full paper.
https://doi.org/10.5194/isprs-annals-X-G-2025-87-2025 | © Author(s) 2025. CC BY 4.0 License.

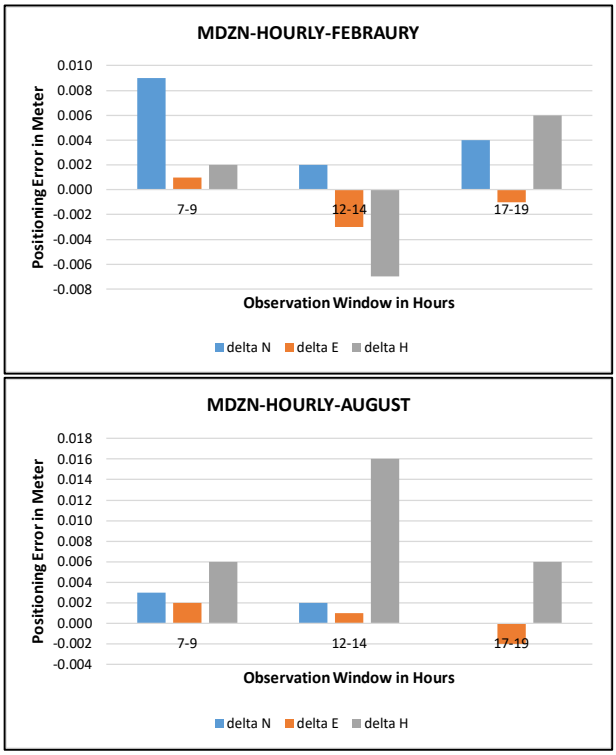

Figure 15. Hourly Error for MDZN station (February & August 2018)

4. Conclusions

This study used the TBC and CSRS-PPP programs to analyze the RINEX data for two Geodetic Reference stations in Abu Dhabi, namely ADCN and MDZN stations, spanning over 2018. Both software programs proved to be robust for GNSS data processing and analysis. The data were successfully analyzed, and the daily trends of the positioning variations in both the horizontal and vertical components were computed. Our results demonstrated small variations and differences between the horizontal and vertical components of both stations and the reference coordinates. The variation at ADCN was slightly larger than that at MDZN, particularly for the vertical component. This could be attributed to the location of both points, as ADCN is located close to the coastline and is more susceptible to the effects of humidity and temperature, whereas MDZN is located in a quiet open environment and away from the coastline.

The impact of the first-order ionospheric delay was successfully removed by the dual-frequency ionosphere-free combination using both the techniques implemented in this study. The remaining error in the station coordinate time series may be attributed to the unresolved residual of higher-order ionospheric error. Furthermore, errors in coordinate estimation may be caused by annual or semi-annual seasonal signatures of the GNSS time series owing to different factors. This can be attributed to systematic errors or certain geodynamic phenomena that should be modeled and removed from the final solution. Other factors affecting accuracy include baseline length, elevation, geoid undulation, slope, land use, GPRS/GSM coverage, and multipath caused by signal blockage from nearby physical structures. Future studies must use more spatially distributed stations with longer observation time series to classify different error types, including ionospheric and tropospheric influences on GNSS accuracy over the United Arab Emirates. Finally, the emergence of new satellite navigation systems, such as the Chinese BeiDou and European Galileo, in addition to the modernization of GPS and GLONASS, will further enhance the PNT accuracy. This requires different survey organizations and academic institutes to upgrade their GNSS receivers to be compatible with all new signals.

Acknowledgements

The United Arab Emirates University is acknowledged for providing the support for this study. We thank Abu Dhabi Municipality for providing the data.

References

Ansari, K., O. Corumluoglu, and S. K. Panda. 2017: Analysis of Ionospheric TEC from GNSS Observables over the Turkish Region and Predictability of IRI and SPIM Models. *Astrophys. Space Sci*., 362 (4), 65. https://doi.org/10.1007/s10509-017-3043-x.

Astudillo, J., L. Lau, Y. Tang, and T. Moore. 2018: Analyzing the Zenith Tropospheric Delay Estimates in On-line Precise Point Positioning (PPP) Services and PPP Software Packages. *Sensors*., 18 (580). https://doi.org/10.3390/s18020580

Awange, J. L. 2012: *Environmental Monitoring Using GNSS: Global Navigation Satellite Systems*. Springer, Heidelberg, Germany.

Brunner, F. K., and W. M. Welsch. 1993: Effect of the Troposphere in GPS Measurements. *GPS World*, 4 (1), 42–51.

Dogan, U., Uludag, M., & Demir, D.O. (2014). Investigation of GPS positioning accuracy during the seasonal variation. Science Direct, measurement 53, 91-100. http://dx.doi.org/10.1016/j.measurement.2014.03.034.

Ebner, R., and W. E. Featherstone. 2008: How Well Can Online GPS PPP Post-Processing Services Be Used To Establish Geodetic Survey Control Networks? *J. Appl. Geod.*, 2 (3), 149–157. https://doi.org/10.1515/JAG.2008.017.

El-Rabbany, A. 2006: *Introduction to GPS: The Global Positioning System*. Artech House Inc., London.

Fernandes, M., J., C. Lazaro, M. Ablain, and N. Pires. 2015: Improved Wet Path Delays for All ESA and Reference Altimetric Missions. *Remote Sens. Environ.*, 169, 50–74. https://doi.org/10.1016/j.rse.2015.07.023

Garrido, M. S., M. C. de Lacy, and A. M. Rojas. 2018: Impact of tropospheric modelling on GNSS vertical precision: An empirical analysis based on a local active network. *Int. J. Digital Earth*, 11 (9), 880–896. https://doi.org/10.1080/17538947.2017.1367040.

Hofmann-Wellenhof, B., H. Lichtenegger, and E. Wasle. 2008: *GNSS: Global Navigation Satellite Systems – GPS, GLONASS, GALILEO & more*. Springer-Verlag press, Wien.

Hong, L. W. 2008: *Interpolation and Mapping of the Total Electron Content Over the Malaysian Region*. Master’s thesis. Universiti Teknologi Malaysia Institutional Repository, Malaysia.

IGS. 2018: *Precise Point Positioning with Ambiguity Resolution (PPP-AR).* https://igs.org/wg/ppp-ar/.

Isioye, O. A., M. Moses, and L. Abdulmumin. 2019: *Comparative Study of Some Online GNSS Post-Processing Services at Selected Permanent GNSS Sites in Nigeria*. In *Accuracy of GNSS methods*. D.U. Sanli (Ed.): IntechOpen, 89-106. https://doi.org/10.5772/intechopen.79924

Jerez, G. O., and D. B. M. Alves. 2020: Assessment of GPS/GLONASS point positioning in Brazilian regions with distinct ionospheric behavior. *Bol. Ciênc. Geod.*, 26 (2), e2020010. https://doi.org/10.1590/s1982-21702020000200010.

Khoptar, A., and S. Savchuk. 2020: Estimation of Ionospheric Delay Influence on the Efficiency of Precise Positioning of Multi-GNSS Observations. *Baltic Surv.*, 12, 14–18. https://doi.org/10.22616/j.balticsurveying.2020.002.

Langley, Richard. 2011: GNSS and the Ionosphere. GPS World, 22 (2), 40–50.

Li, K.-F., L.-C. Lin, X.-H. Bui, and M.-C. Liang. 2018: The 11 Year Solar Cycle Response of the Equatorial Ionization Anomaly Observed by GPS Radio Occultation. *J. Geophys. Res.* Space *Phys*., 123 (1), 848–861. https://doi.org/10.1002/2017JA024634.

Lou, Y. D., W. X. Zhang, C. Wang, X. G. Yao, C. Shi, and J. N. Liu. 2014: The Impact of Orbital Errors on the Estimation of Satellite Clock Errors and PPP. *Adv. Space Res*., 54 (8), 1571–1580. https://doi.org/10.1016/j.asr.2014.06.012.

Łyszkowicz, A., R. Pelc-Mieczkowska, A. Bernatowicz, and S. Savchuk. 2021: First Results of Time Series Analysis of the Permanent GNSS Observations at Polish EPN Stations using GIPSYX Software. *Artif. Satell.*, 56 (3), 101–118. https://doi.org/10.2478/arsa-2021-0008.

NRCan. 2020: *On-line Precise Point Positioning: CSRS-PPP Version 3 Tutorial*. https://webapp.csrs-scrs.nrcan-rncan.gc.ca/geod/tools-outils/sample_doc_filesV3/NRCan%20CSRS-PPP-v3_Tutorial%20EN.pdf.

Petropoulos, G. P., & Srivastava, P. K. (2021). GPS and GNSS technology in geosciences. Elsevier.

Rizos, C. 1997: *Principles and Practice of GPS Surveying.* GMAT5222 course notes. Sydney, NSW: School of Geomatics Engineering, the University of New South Wales. Australia 2052.

Sanlioglu, I., and M. Zeybek. 2012: *Investigation on GPS Heighting Accuracy with Use of Tropospheric Models in Commercial GPS Softwares for Different Heights*. FIG working week 2012. Rome, Italy, 6-10 May 2012.

Shu, B., H. Liu, Y. Feng, L. Xu, C. Qian, and Z. Yang. 2019: Analysis Factors Affecting Asynchronous RTK Positioning with GNSS Signals. *Remote Sens.*, 11 (10), 1256. https://doi.org/10.3390/11.101256.

US- Department of Defense. 2020: *Standard Positioning Service Performance Standard,* 5th Edition. https://www.gps.gov/technical/ps/2020-SPS-performance-standard.pdf.

Yi, W., W. Song, Y. Lou, C. Shi, Y. Yao, H. Guo, M. Chen, and J. Wu. 2017: Improved Method to Estimate Undifferenced Satellite Fractional Cycle Biases using Network Observations to Support PPP Ambiguity Resolution. *GPS Solut.*, 21 (3), 1369–1378. https://doi.org/10.1007/s10291-017-0616-7.